CIRP Journal of Manufacturing Science and Technology 10 (2015) 77–83

Contents lists available at ScienceDirect

CIRP Journal of Manufacturing Science and Technology

journal homepage: www.elsevier.com/locate/cirpj

On the thermal response of a surface deposited laser-irradiated powder particle

T.I. Zohdi *

Department of Mechanical Engineering, University of California, 6117 Etcheverry Hall, Berkeley, CA 94720-1740, USA

ARTICLE INFO

Article history:
Available online 17 June 2015

Keywords:
Powders
Lasers

ABSTRACT

This paper provides a basic analysis of the temperature rise of a particle in a powder that is being irradiated by a laser and simultaneously conducting heat with its surroundings. The work is motivated by the widespread use of laser post-processing of deposited particles in additive manufacturing technologies. The study focuses on one of the "building blocks" of additive, powder-based, technologies, namely the controlled irradiation of a single particle. The analysis employs two models: (a) a classical model, based on a balance of energy in conjunction with Fourier-type conduction and (b) a thermally relaxed model, based on a balance of energy in conjunction with thermally relaxed conduction, which is important when using fast-pulsing lasers. Analytical and numerical results are generated to qualitatively ascertain the time-transient trends as a function of particle size, heat capacity, material density, laser irradiance, conductivity and the thermal relaxation. The objective is to provide researchers with methods to quickly determine the required laser input to bring the particle to a desired temperature, which is an essential step in powder-based additive manufacturing.

1. Introduction

1.1. Motivation

Powder-based additive manufacturing has received a great deal of attention in recent years. We refer the reader to the recent overview article by Huang et al. [1] on the wide array of activities in the manufacturing community in this area. Today, large quantities of inexpensive, high-quality, particles for additive powder-based manufacturing processes, are readily available due to advanced materials processing techniques such as (a) sublimation from a raw solid to a gas, which condenses into particles that are recaptured (harvested), (b) atomization of liquid streams into droplets by breaking jets of metal, (c) reduction of metal oxides and (d) precise comminution/pulverizing of bulk material. Subsequent to the deposition of particles onto a substrate, there are a number of related sub-processes which can make up an overall additive manufacturing process. In particular, oftentimes, one key component is laser processing, which utilizes high-intensity beams to heat particles in a powder to desired temperatures either to subsequently soften, sinter, melt or ablate them. (Fig. 1). Laser-based heating is quite attractive because of the degree of targeted precision that it affords.[1] Because of the monochromatic and collimated nature of lasers, they are an attractive, highly controllable, way to process powdered materials, in particular with pulsing, via continuous beam chopping or modulation of the voltage. For example, Carbon Dioxide (CO_2) and Yttrium Aluminum Garnett (*YAG*) lasers are commonly used. The range of power of a typical industrial laser is relatively wide, ranging from approximately 100–10,000 W. Typically, the initial beam produced is in the form of collimated (parallel) rays that are 1–2 mm apart, which are then focussed with a lens onto a small focal point (approximately 50 mm away) of no more than about 0.00001 m in diameter. *However*, one concern of manufacturers are the microstructural defects generated in additively manufactured products, created by imprecisely controlled heat affected zones, brought on by miscalibration of the laser power needed for a specific goal. For example, due to the rise of one family of additive manufacturing, printed flexible electronics, involving sensitive

[1] There are a variety of other techniques that may be involved in an overall additive manufacturing processes, such as: (a) electron beam melting, which is a process by where metal powder is bonded together layer per layer with an electron beam in a high vacuum, (b) aerosol jetting, which consists of utilizes directing streams of atomized particles at high velocities towards a substrate and (c) inkjet printing, which works by projecting small droplets of ink towards a substrate through a small orifice by pressure, heat, and vibration. The deposited materials is then heated by UV light or other means to rapidly dry.

* Tel.: +1 5106429172.
E-mail address: zohdi@berkeley.edu

http://dx.doi.org/10.1016/j.cirpj.2015.05.001
1755-5817/

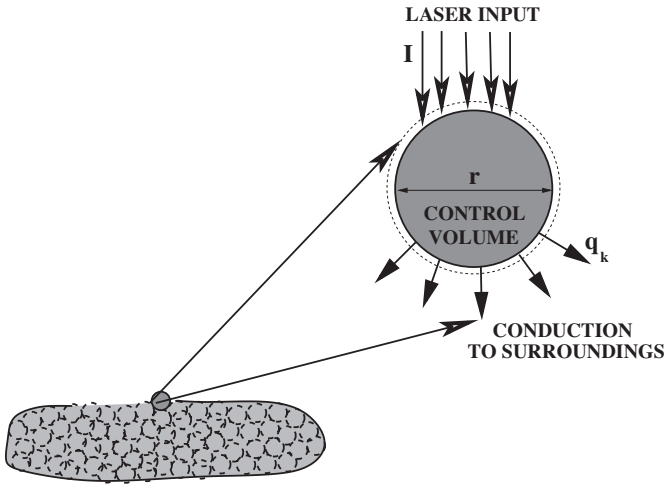

Fig. 1. A schematic of laser input applied to a particle control volume.

substrates, it is important to precisely understand how much laser-input is needed. Furthermore, in many cases one may need to pulse the laser, either for technological reasons, such as to avoid overheating, or to activate certain thermal relaxation effects, which are discussed later. In particular, because many substrates can become thermally damaged, for example from thermal stresses, ascertaining the appropriate amount of laser input is necessary. Applications include, for example, optical coatings and photonics (Nakanishi et al. [2]), MEMS applications (Fuller et al. [3], Samarasinghe et al. [4] and Gamota et al. [5]) and Biomedical devices (Ahmad et al. [6]). In terms of processing techniques, we refer the reader to Sirringhaus et al. [7], Wang et al. [8], Huang et al. [9], Choi et al. [10–13] and Demko et al. [14,15] for details. Thus, in order for *emerging additive approaches to succeed, one must draw upon rigorous theory and computation to guide and simultaneously develop design rules for upscaling to industrial manufacturing levels. This motivates the present analysis.*

Remark: In 2014, related print-like additive manufacturing technologies, employing deposition of particulate materials, including ceramics, metals, plastics, organic, and even biological materials was a 2.2 billion dollar industry, with applications ranging from commercial manufacturing, medical technology, art and academia.[2] These types of applications and associated technology are closely related to those in the area spray coatings, and we refer the reader to the extensive works of Sevostianov and Kachanov [16–18], Nakamura and coworkers: Dwivedi et al. [19], Liu et al. [20,21], Nakamura and Liu [22], Nakamura et al. [23] and Qian et al. [24] and to Martin [25,26] for the state of the art in deposition technologies.

1.2. Scientific objectives

The objective of this paper is to study one of the "building blocks" of additive, powder-based, technologies, namely the irradiation of a single particle. We first analytically study the terms that contribute to achieving a target temperature by constructing an energy balance on a control volume accounting for incoming laser irradiance and heat conduction to the body. During the course of the analysis, key parameter groups are identified in order to determine the relative contribution of each type of physics. Numerical examples are provided to illustrate the model's behavior. The framework is, by design, straightforward to computationally implement, in order to be easily utilized by researchers in the field. Importantly, we note that within the last decade, technological advances have enabled the reliable control of ultrafast pulsed lasers to activate small-time scale heat wave effects. These effects are often referred to as thermally relaxed "second-sound" effects, because of their mathematical similarity to wave propagation in acoustics, although normal sound waves are fluctuations in the density of molecules in a substance while thermally relaxed second-sound waves are fluctuations in the density of phonons. Such phenomena are predicted by models which introduce thermal relaxation times into heat-conduction relations. The thermally relaxed second-sound is a quantum mechanical phenomenon in which heat transfer occurs by wave-like motion, rather than by the more usual mechanism of diffusion. This leads to a very high confinement of thermal energy in very targeted zones. Thermally relaxed phenomena can be observed in any system in which most phonon–phonon collisions conserve momentum, and can play a role when the time scale of heat input is quite small. The analysis proceeds by generating results for the response of an irradiated particle, as a function of particle size, heat capacity, material density, laser irradiance, conductivity and thermal relaxation, based on a balance of energy in conjunction with two models: (a) a classical Fourier-type conduction model and (b) a thermally relaxed model. Analytical and numerical results are generated to qualitatively ascertain the time-transient trends as a function of particle size, heat capacity, material density, laser irradiance, conductivity and the thermal relaxation. Furthermore, a numerical scheme is also developed to solve the governing equations for general laser input.

Remark: The additive dynamic deposition process of multibody and inter-particle collisions that occurs before the irradiation by a laser is outside the scope of the present work. We refer the reader to Duran [28], Pöschel and Schwager [29], Onate et al. [30–32], Rojek et al. [33,34], Carbonell et al. [35], Labra and Onate [36], Leonardi et al. [37], Cante et al. [38], Bolintineanu et al. [39], Avci and Wriggers [40] and Zohdi [41–51] for more computationally-oriented techniques aligned with manufacturing processes involving particles.

2. Thermal relaxation/second-sound effects

2.1. Continuum model

The thermally relaxed second-sound type model can be motivated by a Jeffreys-type relation between the conductive flux and temperature gradient (Joseph amd Preziosi [52]):

$$\tau \frac{\partial \boldsymbol{q}_k}{\partial t} + \boldsymbol{q}_k = -\mathbf{IK} \cdot \nabla \theta, \tag{2.1}$$

where τ is the relaxation time, θ is the temperature, t is time, $\boldsymbol{q}_k$ is the conductive heat flux, **IK** is the thermal conductivity. A balance of power reads

$$\rho C \frac{\partial \theta}{\partial t} = -\nabla \cdot \boldsymbol{q}_k - \nabla \cdot \boldsymbol{q}_o, \tag{2.2}$$

where ρ is the mass density, C is the heat capacity and $\boldsymbol{q}_o$ is the flux due to other sources, such as laser energy input. By taking the partial derivative with respect to time of the above yields, assuming no material changes,

$$\rho C \frac{\partial^2 \theta}{\partial t^2} = -\frac{\partial (\nabla \cdot \boldsymbol{q}_k + \nabla \cdot \boldsymbol{q}_o)}{\partial t} = -\nabla \cdot \left(\frac{\partial \boldsymbol{q}_k}{\partial t} + \frac{\partial \boldsymbol{q}_o}{\partial t} \right). \tag{2.3}$$

[2] A rough market percentage breakdown is 30 % motor vehicles, 15 % consumer products, business 11 %, medical 9 % and 35 % spread across other fields. Three-dimensional printing was pioneered in 1984 by Hull [27] of the 3D-Systems Corporation.

Inserting Eq. (2.1) into (2.2) and 2.3 yields

$$\frac{\partial^2\theta}{\partial t^2}+\frac{1}{\tau}\frac{\partial\theta}{\partial t}=\frac{1}{\rho C\tau}\nabla\cdot\mathbf{IK}\cdot\nabla\theta-\frac{1}{\rho C\tau}\nabla\cdot\boldsymbol{q}_o-\frac{1}{\rho C}\nabla\cdot\frac{\partial\boldsymbol{q}_o}{\partial t}. \tag{2.4}$$

This produces attenuating heat waves. In the case of a homogeneous medium, the wave speed is $\sqrt{\frac{\mathbf{IK}}{\rho C\tau}}$.

2.2. Extreme cases

We have the following extreme parameter cases:

- In the special case of $\tau\to 0$, one obtains the classical heat conduction equation

$$\rho C\frac{\partial\theta}{\partial t}=\nabla\cdot\mathbf{IK}\cdot\nabla\theta-\nabla\cdot\boldsymbol{q}_o. \tag{2.5}$$

- In the special case of $\tau\to\infty$, one obtains

$$\rho C\frac{\partial^2\theta}{\partial t^2}=-\nabla\cdot\frac{\partial\boldsymbol{q}_o}{\partial t}=-\frac{\partial}{\partial t}\nabla\cdot\boldsymbol{q}_o, \tag{2.6}$$

  which eliminates heat losses due to conduction, thus confining heat input.
- In the special case when $\tau\to\infty$, $\mathbf{IK}\to\infty$ and $\frac{\mathbf{IK}}{\tau}$ remaining finite, then a purely hyperbolic equation arises

$$\frac{\partial^2\theta}{\partial t^2}=\frac{1}{\rho C\tau}\nabla\cdot\mathbf{IK}\cdot\nabla\theta \tag{2.7}$$

An excellent review of a wide range of heat transfer models can be found in the seminal review paper of Joseph and Preziosi [52].

3. Reduced-order model

In order to simplify the analysis for a single particle, we consider a lumped mass model shown in Fig. 1 (a control volume inside the dashed lines). We remark that the validity of using a lumped thermal model for a particle, i.e. ignoring temperature gradients and assuming a uniform temperature within a particle, is dictated by the magnitude of the Biot number. A small Biot number (significantly less than unity) indicates that such an approximation is reasonable. The Biot number for spheres scales with the ratio of particle volume ($V=\frac{4}{3}\pi r^3$) to particle surface area ($A_S=4\pi r^2$), $\frac{V}{A_S}=\frac{r}{3}$ (r is the particle radius), which indicates that a uniform temperature distribution is appropriate, since the particle, by definition, is small. The governing equation, given by an overall energy balance (First Law of Thermodynamics), for the thermally relaxed model is

$$\ddot{\theta}+\frac{1}{\tau}\dot{\theta}=\frac{\mathrm{IK}A_S}{MCh\tau}(\theta_S-\theta)+\frac{(1-R)I^i(t)A_L}{MC\tau}+\frac{A_L}{MC}\times\frac{d((1-R)I^i(t))}{dt}, \tag{3.1}$$

where M is the mass of the particle and h is a length-scale for conduction (essentially the radius of the particle). For the classical Fourier case we have

$$\dot{\theta}=\frac{\mathrm{IK}A_S}{MCh}(\theta_S-\theta)+\frac{(1-R)I^i(t)A_L}{MC}. \tag{3.2}$$

- Note that the absorbed incident optical radiation is: $I^a(t)A_L=(I^i-I^r)A_L=(1-R)I^iA_L$, where I^a is the absorbed radiation per unit area, $I^r=RI^i$ is the reflected radiation, R is the reflectivity, $I^i=P/A_B$ is the incident radiation per unit area, P being the power (Watts), A_B is the area of the beam and A_L is the area of the exposed (laser irradiated) surface.
- Note that the conduction to the surroundings is: $\frac{\mathrm{IK}}{h}(\theta_S-\theta)A_S$, where θ is the temperature of the material to be removed, θ_S is the temperature of the body to which the material is attached, A_S is the area of the surrounding surface that conducts heat, IK is the effective conductivity and h is the length scale over which the conduction occurs, which will be taken to be the radius of the particle.

4. Solution character

4.1. Thermal relaxation/second-sound model

Let us put the thermally relaxed second-sound equation in the classical form:

$$\ddot{\theta}+2\zeta\omega_n\dot{\theta}+\omega_n^2\theta=f(t), \tag{4.1}$$

where

- $\omega_n=\sqrt{\frac{\mathrm{IK}A_S}{\tau hMC}}$,
- $\tau=\frac{1}{2\zeta\omega_n}$, thus $\zeta=\frac{1}{2}\sqrt{\frac{hMC}{\mathrm{IK}A_S\tau}}$,
- $f(t)=\frac{(1-R)I^i(t)A_L}{MC\tau}+\frac{A_L}{MC}\frac{d(1-R)I^i(t)}{dt}+\frac{\mathrm{IK}A_S}{\tau hMC}\theta_S$.

This is the form of a forced damped oscillator. Depending on the value of ζ, the solution will have one of three distinct types of behavior:

- $\zeta>1$, overdamped, leading to no oscillation, where the value of θ approaches equilibrium for large values of time.
- $\zeta=1$, critically damped, leading to no oscillation, where the value of θ approaches equilibrium for large values of time, however faster than the overdamped solution.
- $\zeta<1$, underdamped, leading to damped oscillation, where the value of θ approaches equilibrium for large values of time, in an oscillatory fashion.

Thus, clearly, such systems could resonate if forced at certain frequencies.

4.2. Asymptotics as $\tau\to 0$

As indicated earlier, as $\tau\to 0$, we recover the classical model:

$$MC\dot{\theta}=(1-R)I^iA_L+\frac{\mathrm{IK}A_S}{h}(\theta_S-\theta), \tag{4.2}$$

which for simple cases can be solved analytically, for example for a constant laser input $I^i(t)=I^i$ (assuming $\theta(t=0)=\theta_S$)

$$\theta(t)=\theta_S+\frac{(1-R)I^iA_Lh}{\mathrm{IK}A_S}\left(1-e^{-\frac{\mathrm{IK}A_St}{MCh}}\right). \tag{4.3}$$

The relation above is important since it provides a qualitative relation that connects the temperature, to the laser input, conductivity, contact area and time. For example, if one set the desired temperature at a desired time to be $\theta(t^*)=\theta^*$ one can solve for the laser input needed

$$I^{*,i}=\frac{(\theta^*-\theta_S)\mathrm{IK}A_S}{(1-R)A_Lh\left(1-e^{-\frac{\mathrm{IK}A_St^*}{MCh}}\right)}. \tag{4.4}$$

4.3. Observations

We have the following observations:

- The rise time for the temperature is dictated by the ratio of conduction to heat capacity, $\frac{\mathrm{IK}A_S}{MCh}$.
- At steady-state, $e^{-\frac{\mathrm{IK}A_St}{MCh}}\to 0$, and

$$\theta(t) = \theta_S + \frac{(1-R)I^i A_L h}{\mathrm{IK}A_S}, \tag{4.5}$$

which indicates that the ratio of $I^a = (1-R)I^i$ to $\frac{\mathrm{IK}}{h}$ dictates the steady state temperature (assuming $A_L \approx A_S$).

- For a highly conductive surrounding: $\mathrm{IK} \to \infty$, $\theta(t) = \theta_S$, where the conductive losses are instantaneous. This will draw heat away from the targeted zone.
- For a poorly conductive surrounding: $\mathrm{IK} \to 0$, $\theta(t) = \theta_S + \frac{(1-R)I^i A_L t}{MC}$, where the conductive losses are zero. This will trap (maximize) heat in the targeted zone.
- For the thermally relaxed model, as $\tau \to \infty$, one obtains

$$\frac{\partial}{\partial t}\left(\frac{\partial \theta}{\partial t} - \frac{A_L}{MC}(1-R)I^i(t)\right) = 0. \tag{4.6}$$

The integral solution of this equation is

$$\begin{aligned}\theta(t) &= \theta(t \\ &= 0) + \frac{A_L}{MC}\int_0^T (1-R)I^i(t)\,dt \\ &+ \left(\dot\theta(t=0) - \frac{A_L(1-R)I^i(t=0)}{MC}\right)t\end{aligned} \tag{4.7}$$

In the usual case when $\dot\theta(t=0) = \frac{A_L(1-R)I^i(t=0)}{MC}$, we have

$$\theta(t) = \theta(t=0) + \frac{A_L}{MC}\int_0^T (1-R)I^i(t)\,dt, \tag{4.8}$$

which yields the same solution as for **IK** = 0.

4.4. Order of magnitude analysis

The ratios of the contributing terms are, leaving the dimensions of the target and the laser-power as variables:

$$\begin{aligned}\frac{CONDUCTION}{LASER-IRRAD.} &= \frac{\mathrm{IK}(\theta_S - \theta)A_S}{h(1-R)I^i A_L} \approx \frac{\mathcal{O}(10^2)\mathcal{O}(10^2)A_S}{(1-R)I^i A_L h} \\ &\approx \frac{\mathcal{O}(10^4)}{(1-R)I^i h},\end{aligned} \tag{4.9}$$

where the ratio of the areas is assumed to be of order unity($A_L \approx A_S$). Rewriting the irradiance per unit area in terms of power input, $(1-R)I^I = \frac{P}{A_L}$, yields

$$\frac{CONDUCTION}{LASER-IRRAD.} \approx \frac{\mathcal{O}(10^4)}{P\frac{h}{A_L}}, \tag{4.10}$$

and thus since $A_L \propto \pi h^2$ (h is effectively the radius of the particle)

$$\frac{CONDUCTION}{LASER-IRRAD.} \approx \frac{\mathcal{O}(10^4)h}{P}. \tag{4.11}$$

For example, for an idealized spherical particle, we have (Fig. 1)

- $A_S = \beta 4\pi r^2$, where $0 \le \beta \le 1$,
- $A_L = \pi r^2$.

For $r \approx h$, this yields $\frac{A_L}{h} \approx \mathcal{O}(r)$. Thus, for a small target, for example $r \approx 10^{-3}$ meters, $P \approx 10^3$ *Watts*, then

$$\frac{CONDUCTION}{LASER-IRRAD.} \approx \mathcal{O}(10^{-2}). \tag{4.12}$$

Thus, the laser input is 100 times larger that conduction.

5. Numerical solution scheme

Although the solution to the thermally relaxed second-sound equation can be solved analytically for most cases involving simple constant irradiation loadings, we none-the-less generated a simple forward-Euler scheme to consider general pulsed loading. For the thermally relaxed equation, we have

$$\frac{\theta(t+\Delta t) - \theta(t)}{\Delta t} \approx \dot\theta(t) \Rightarrow \theta(t+\Delta t) \approx \theta(t) + \Delta t\dot\theta(t) \tag{5.1}$$

where

$$\begin{aligned}\frac{\dot\theta(t) - \dot\theta(t-\Delta t)}{\Delta t} + \frac{1}{\tau}\dot\theta(t-\Delta t) &= \frac{\mathrm{IK}A_S}{MCh\tau}(\theta_S - \theta(t-\Delta t)) \\ &+ \frac{(1-R)I^i(t-\Delta t)A_L}{MC\tau} + \frac{A_L}{MC} \\ &\times \frac{\mathrm{d}(1-R)I^i(t-\Delta t)}{\mathrm{d}t}\end{aligned} \tag{5.2}$$

yields

$$\begin{aligned}\dot\theta(t) &= \Delta t\left(\dot\theta(t-\Delta t)\left(\frac{1}{\Delta t} - \frac{1}{\tau}\right) + \frac{\mathrm{IK}A_S}{MCh\tau}(\theta_S - \theta(t-\Delta t))\right) \\ &+ \Delta t\left(\frac{(1-R)I^i(t-\Delta t)A_L}{MC\tau} + \frac{A_L}{MC}\frac{\mathrm{d}(1-R)I^i(t-\Delta t)}{\mathrm{d}t}\right).\end{aligned} \tag{5.3}$$

For the classical conduction equation, the scheme is simply

$$\theta(t+\Delta t) = \theta(t) + \Delta t\left(\frac{IKA_S}{MCh}(\theta_S - \theta(t)) + \frac{(1-R)I^i(t)A_L}{MC}\right). \tag{5.4}$$

For either model, the algorithm is to step the solution forward in time, update the temperature then repeating until the end of the specified simulation time.

6. Examples

We considered one of the most commonly used pulsed laser inputs, namely a repetitive Heaviside beam (Fig. 2), which can written mathematically as:

$$I^i(t) = I_o, \quad \text{if } t^{(-)} \le t \le t^{(+)} \tag{6.1}$$

and

$$I^i(t) = 0, \quad \text{otherwise}, \tag{6.2}$$

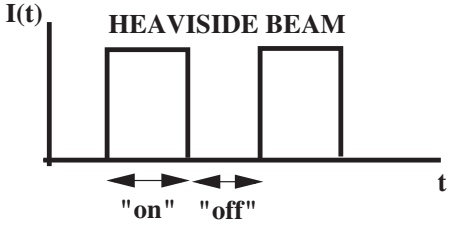

Fig. 2. A pulsed Heaviside beam used in the example.

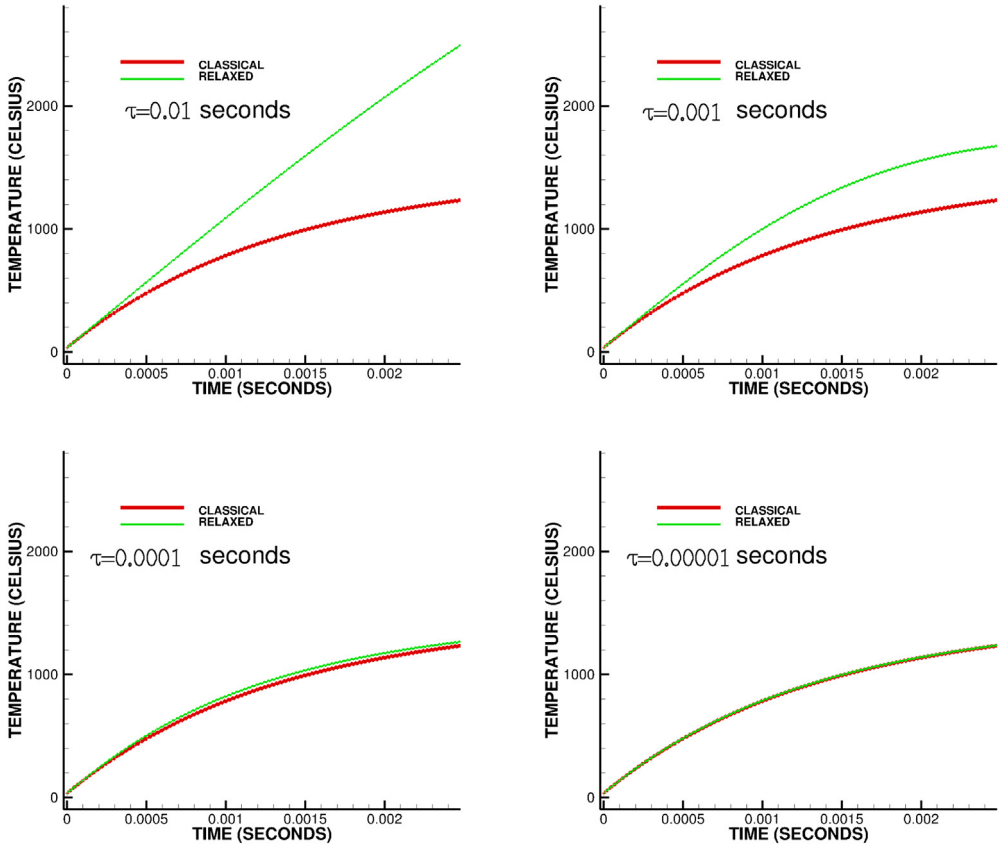

Fig. 3. An example: The temperature of the particle as a function of time for $P_o = 1000$ W and (top-left) $\tau = 0.01$ s, (top-right) $\tau = 0.001$ s, (bottom-left) $\tau = 0.0001$ s and (bottom-right) $\tau = 0.00001$ s. All results are compared against the $\tau = 0$ s (classical Fourier conduction) case (lower valued red line). (For interpretation of the references to color in this figure legend, the reader is referred to the web version of the article.)

with repetition as needed.[3] For each pulse, the selected time "on" was $\delta t = 1.5 \times 10^{-5}$ seconds and the time "off" was $\delta t = 10^{-5}$ seconds as well.

The other input parameters used were:

- Radius: $r = 0.001$ m,
- Initial surrounding temperature: $\theta_S = 30$ °C,
- Starting particle temperature: $\theta(t) = 30$ °C,
- Initial particle temperature rate: $\dot{\theta}(t = 0) = 0$ °C/s,
- Laser beam radius: $r_B = 0.001$ m yields laser beam area $A_B = \pi r_B^2$ m^2,
- Effective reflectivity of the particle: $R = 0.25$,
- Nominal power: $P_o = 1000$ W yields the irradiance per unit area, $I_o = \frac{P_o}{A_B}$ W/m^2, where the absorbed irradiance is $I^a = (1 - R)\frac{P_o}{A_B}$ W/m^2,
- Density: $\rho = 1000$ kg/m^3,
- Conductivity: IK = 100 W/m – °C,
- Heat capacity: $C = 100$ J/kg – °C,
- Thermal relaxation: $\tau = 0.01$, $\tau = 0.001$, $\tau = 0.0001$ and $\tau = 0.00001$ s,
- Conductive area: $\beta \times 4\pi r^2$ m^2, where $\beta = 0.5$ and
- Numerical time step size: $\Delta t = 0.0000001$ s.

100 on-off pulses were used for a resulting total simulation time of $T = 0.0025$ *s*. Also, for the purposes of illustration, the temperature of the surrounding around the particle was parametrized via

$$\theta_S = \gamma\theta(t) + (1 - \gamma)\theta_S(t = 0), \tag{6.3}$$

where $(0 \leq \gamma \leq 1)$ the two extremes are:

- $\gamma = 1$ induces a state where there is no conduction, since $\theta_S = \theta(t)$,
- $\gamma = 0$ induces a state where the surrounding's temperature is controlled to be the initial temperature.

The simple parametrization allows one to explore the extremes associated with the surrounding environment ($\gamma = 0.5$ was selected).

The general trends in Fig. 3 indicate the temperature versus time as a function of τ. In all cases, the temperature with the relaxed model is higher than that predicted by the classical model, due to the fact that the heat remains confined. The time-stepping discretization parameter (Δt) was made sufficiently small so that the results were insensitive to further time-step size reductions. In other words, the depicted numerical results are essentially free of numerical error.[4] The approach provides researchers in the field to quickly assess how much power input is needed to drive a system to a prespecified temperature, which is an essential first step in powder-based additive manufacturing. The current analysis does not include phase-transformations and latent heat terms used to describe subsequent softening, melting or ablation. The extension of this analysis to those regimes is discussed next.

7. Summary and extensions

In summary, this paper provided an analysis of the thermal response of a generic particle being irradiated by a laser and conducting heat with its surroundings. Two models were studied: (a) a classical model, based on a balance of energy in conjunction

[3] A continuous beam is simply $I^i(t) = I_o$.

[4] For several benchmark problems, for constant loadings, the numerical and analytical solution were generated in complete agreement.

with Fourier-type conduction and (b) a thermally relaxed model, based on a balance of energy in conjunction with thermally relaxed conduction. Both analytical and numerical results were generated. The practical use of a relaxation model (employing τ) would be to:

1. Solve the mathematical system with $\tau = 0$, and to generate the solution, denoted $\theta^{\tau=0}$,
2. Compare the result to temperatures generated by experiments, θ^{ex} and
3. Re-solve the mathematical problem with a series of τ's until one achieves the closest match possible to the experimental temperature.

To reliably extend this work, the spatial propagation of the thermal fields through conduction, as well as phase-transformations, are of interest, and require the use of spatial discretization techniques such as the Discrete Element Method, the Finite Difference Method or the Finite Element Method. Furthermore, an aspect of key interest is the characterization of the dynamic deposition of the powder, as well as potentially hazardous particulate ejecta induced by laser processing. To describe both processes, Discrete Element Methods are ideal, whereby relatively simple, physically meaningful, multibody dynamics models for many interacting particles comprising powder are used and their changes of phase from a solid, to a liquid to a gas are tracked, particle by particle.[5] For example, using the Discrete Element Method, Zohdi [47,51] has developed a computational model and corresponding solution algorithm for the rapid simulation of the laser processing and targeted localized heating of materials composed of discrete particles that are packed together. The discrete element model captures the main physical effects through (1) a discretization of a concentrated laser beam into rays, (2) a discrete element representation of the particulate material microstructure and (3) a discrete element transient heat transfer model that accounts for optical (laser) energy propagation (reflection and absorption), its conversion into heat. An extension of this model to include phase transformations involving melting and vaporization and the debris ejecta is currently underway by the author. It is important to note that many of the processes involve multiple stages of nonmonotone evaporative heating and cooling, and mass transfer.

References

[1] Huang, Y., Leu, M.C., Mazumdar, J., Donmez, A., 2015, Additive Manufacturing: Current State, Future Potential, Gaps and Needs, and Recommendation, Journal of Manufacturing Science and Engineering, 137. 014001-1.

[2] Nakanishi, H., Bishop, K.J.M., Kowalczyk, B., Nitzan, A., Weiss, E.A., Tretiakov, K.V., Apodaca, M.M., Klajn, R., Stoddart, J.F., Grzybowski, B.A., 2009, Photoconductance and Inverse Photoconductance in Thin Films of Functionalized Metal Nanoparticles, Nature, 460:371–375.

[3] Fuller, S.B., Wilhelm, E.J., Jacobson, J.M., 2002, Ink-Jet Printed Nanoparticle Microelectromechanical Systems, Journal of Microelectromechanical Systems, 11:54–60.

[4] Samarasinghe, S.R., Pastoriza-Santos, I., Edirisinghe, M.J., Reece, M.J., Liz-Marzan, L.M., 2006, Printing Gold Nanoparticles with an Electrohydrodynamic Direct Write Device, Gold Bulletin, 39:48–53.

[5] Gamota, D., Brazis, P., Kalyanasundaram, K., Zhang, J., 2004, Printed Organic and Molecular Electronics, Kluwer Academic Publishers, New York.

[6] Ahmad, Z., Rasekh, M., Edirisinghe, M., 2010, Electrohydrodynamic Direct Writing of Biomedical Polymers and Composites, Macromolecular Materials and Engineering, 295:315–319.

[7] Sirringhaus, H., Kawase, T., Friend, R.H., Shimoda, T., Inbasekaran, M., Wu, W., Woo, E.P., 2000, High-Resolution Inkjet Printing of All-Polymer Transistor Circuits, Science, 290:2123–2126.

[8] Wang, J.Z., Zheng, Z.H., Li, H.W., Huck, W.T.S., Sirringhaus, H., 2004, Dewetting of Conducting Polymer Inkjet Droplets on Patterned Surfaces, Nature Materials, 3:171–176.

[9] Huang, D., Liao, F., Molesa, S., Redinger, D., Subramanian, V., 2003, Plastic-Compatible Low-Resistance Printable Gold Nanoparticle Conductors for Flexible Electronics, Journal of the Electrochemical Society, 150/7: G412–G417.

[10] Choi, S., Park, I., Hao, Z., Holman, H.Y., Pisano, A.P., Zohdi, T.I., 2010, Ultra-Fast Self-Assembly of Micro-Scale Particles by Open Channel Flow, Langmuir, 26/7: 4661–4667.

[11] Choi, S., Stassi, S., Pisano, A.P., Zohdi, T.I., 2010, Coffee-Ring Effect-Based Three Dimensional Patterning of Micro/Nanoparticle Assembly with a Single Droplet, Langmuir, 26/14: 11690–11698.

[12] Choi, S., Jamshidi, A., Seok, T.J., Zohdi, T.I., Pisano, A.P., 2012, Fast, High-Throughput Creation of Size-Tunable Micro, Nanoparticle Clusters Via Evaporative Self-Assembly in Picoliter-Scale Droplets of Particle Suspension, Langmuir, 28/6: 3102–3111.

[13] Choi, S., Pisano, A.P., Zohdi, T.I., 2013, An Analysis of Evaporative Self-Assembly of Micro Particles in Printed Picoliter Suspension Droplets, Journal of Thin Solid Films, 537/30: 180–189.

[14] Demko, M., Choi, S., Zohdi, T.I., Pisano, A.P., 2012, High Resolution Patterning of Nanoparticles by Evaporative Self-Assembly Enabled by In-situ Creation and Mechanical Lift-off of a Polymer Template, Applied Physics Letters, 99:253102-1–253102-3.

[15] Demko, M.T., Cheng, J.C., Pisano, A.P., 2010, High-Resolution Direct Patterning of Gold Nanoparticles by the Microfluidic Molding Process, Langmuir, 412–417.

[16] Sevostianov, I., Kachanov, M., 2000, Modeling of the Anisotropic Elastic Properties of Plasma-Sprayed Coatings in Relation to Their Microstructure, Acta Materialia, 48/6: 1361–1370.

[17] Sevostianov, I., Kachanov, M., 2001, Thermal Conductivity of Plasma Sprayed Coatings in Relation to Their Microstructure, Journal of Thermal Spray Technology, 9/4: 478–482.

[18] Sevostianov, I., Kachanov, M., 2001, Plasma-Sprayed Ceramic Coatings: Anisotropic Elastic and Conductive Properties in Relation to the Microstructure, Cross-Property Correlations Materials Science and Engineering-A v, 297:235–243.

[19] Dwivedi, G., Wentz, T., Sampath, S., Nakamura, T., 2010, Assessing Process and Coating Reliability Through Monitoring of Process and Design Relevant Coating Properties, Journal of Thermal Spray Technology, 19:695–712.

[20] Liu, Y., Nakamura, T., Dwivedi, G., Valarezo, A., Sampath, S., 2008, Anelastic Behavior of Plasma Sprayed Zirconia Coatings, Journal of American Ceramic Society, 91:4036–4043.

[21] Liu, Y., Nakamura, T., Srinivasan, V., Vaidya, A., Gouldstone, A., Sampath, S., 2007, Nonlinear Elastic Properties of Plasma Sprayed Zirconia Coatings and Associated Relationships to Processing Conditions, Acta materialia, 55:4667–4678.

[22] Nakamura, T., Liu, Y., 2007, Determination of Nonlinear Properties of Thermal Sprayed Ceramic Coatings via Inverse Analysis, International Journal of Solids and Structures, 44:1990–2009.

[23] Nakamura, T., Qian, G., Berndt, C.C., 2000, Effects of Pores on Mechanical Properties of Plasma Sprayed Ceramic Coatings, Journal of American Ceramic Society, 83:578–584.

[24] Qian, G., Nakamura, T., Berndt, C.C., 1998, Effects of Thermal Gradient and Residual Stresses on Thermal Barrier Coating Fracture, Mechanics of Materials, 27:91–110.

[25] Martin, P., 2009, Handbook of Deposition Technologies for Films and Coatings, 3rd ed. Elsevier.

[26] Martin, P., 2011, Introduction to Surface Engineering and Functionally Engineered Materials. Scrivener and Elsevier, Journal of Vacuum Science and Technology, A2/2: 500.

[27] Hull, C. (1984). Apparatus for Production of Three-Dimensional Objects by Stereolithography. U.S. Patent 4,575,330.

[28] Duran, J., 1997, Sands, powders and grains. An introduction to the physics of Granular Matter, Springer Verlag.

[29] Pöschel, T., Schwager, T., 2004, Computational Granular Dynamics, Springer Verlag..

[30] Onate, E., Idelsohn, S.R., Celigueta, M.A., Rossi, R., 2008, Advances in the Particle Finite Element Method for the Analysis of Fluid-Multibody Interaction and Bed Erosion in Free Surface Flows, Computer Methods in Applied Mechanics and Engineering, 197/19-20: 1777–1800.

[31] Onate, E., Celigueta, M.A., Idelsohn, S.R., Salazar, F., Suárez, B., 2011, Possibilities of the Particle Finite Element Method for Fluid-Soil-Structure Interaction Problems, Computational Mechanics, 48:307–318.

[32] Onate, E., Celigueta, M.A., Latorre, S., Casas, G., Rossi, R., Rojek, J., 2014, Lagrangian Analysis of Multiscale Particulate Flows with the Particle Finite Element Method, Computational Particle Mechanics, 1/1: 85–102.

[33] Rojek, J., Labra, C., Su, O., Onate, E., 2012, Comparative Study of Different Discrete Element Models and Evaluation of Equivalent Micromechanical Parameters, International Journal of Solids and Structures, 49:1497–1517. http://dx.doi.org/10.1016/j.ijsolstr.2012.02.032.

[34] Rojek, J., 2014, Discrete Element Thermomechanical Modelling of Rock Cutting with Valuation of Tool Wear, Computational Particle Mechanics, 1/1: 71–84.

[35] Carbonell, J.M., Onate, E., Suarez, B., 2010, Modeling of Ground Excavation with the Particle Finite Element Method, Journal of Engineering Mechanics ASCE, 136:455–463.

[5] Such materials possess a complex microstructure which contains gaps and interfaces. This type of process is extremely difficult to simulate using continuum-based methods, such as the Finite Difference Method or the Finite Element Method.

[36] Labra, C., Onate, E., 2009, High-Density Sphere Packing for Discrete Element Method Simulations, Communications in Numerical Methods in Engineering, 25/7: 837–849.
[37] Leonardi, A., Wittel, F.K., Mendoza, M., Herrmann, H.J., 2014, Coupled DEM-LBM Method for the Free-Surface Simulation of Heterogeneous Suspensions, Computational Particle Mechanics, 1/1: 3–13.
[38] Cante, J., Davalos, C., Hernandez, J.A., Oliver, J., Jonsen, P., Gustafsson, G., Haggblad, H.A., 2014, PFEM-Based Modeling of Industrial Granular Flows, Computational Particle Mechanics, 1/1: 47–70.
[39] Bolintineanu, D.S., Grest, G.S., Lechman, J.B., Pierce, F., Plimpton, S.J., Schunk, P.R., 2014, Particle Dynamics Modeling Methods for Colloid Suspensions, Computational Particle Mechanics, 1/3: 321–356.
[40] Avci, B., Wriggers, P., 2012, A DEM-FEM Coupling Approach for the Direct Numerical Simulation of 3D Particulate Flows, Journal of Applied Mechanics, 79:010901–010907.
[41] Zohdi, T.I., 2003, Genetic Design of Solids Possessing a Random-Particulate Microstructure, Philosophical Transactions of the Royal Society: Mathematical Physical and Engineering Sciences, 361/1806: 1021–1043.
[42] Zohdi, T.I., 2003, On the Compaction of Cohesive Hyperelastic Granules at Finite Strains, Proceedings of the Royal Society, 454/2034: 1395–1401.
[43] Zohdi, T.I., 2004, A Computational Framework for Agglomeration in Thermo-chemically Reacting Granular Flows, Proceedings of the Royal Society, 460/2052: 3421–3445.
[44] Zohdi, T.I., 2012, Estimation of Electrical-Heating Load-Shares for Sintering of Powder Mixtures, Proceedings of the Royal Society, 468:2174–2190.
[45] Zohdi, T.I., 2012, Dynamics of charged particulate systems. Modeling, theory and computation, Springer-Verlag.
[46] Zohdi, T.I., 2013, Numerical Simulation of Charged Particulate Cluster-Droplet Impact on Electrified Surfaces, Journal of Computational Physics, 233:509–526.
[47] Zohdi, T.I., 2013, Rapid Simulation of Laser Processing of Discrete Particulate Materials, Archives of Computational Methods in Engineering, 1–17. 10.1007/s11831-013-9092-6.
[48] Zohdi, T.I., 2014, A Direct Particle-Based Computational Framework for Electrically-Enhanced Thermo-mechanical Sintering of Powdered Materials, Mathematics and Mechanics of Solids, 1–21. 10.1007/s11831-013-9092-6..
[49] Zohdi, T., 2014, Embedded Electromagnetically Sensitive Particle Motion in Functionalized Fluids, Computational Particle Mechanics, 1/1: 27–45.
[50] Zohdi, T.I., 2014, Rapid Computation of Statistically-Stable Particle/Feature Ratios for Consistent Substrate Stresses in Printed Flexible Electronics, Journal of Manufacturing Science and Engineering ASME, . http://dx.doi.org/10.1115/1.4029327. MANU-14-1476.
[51] Zohdi, T.I., 2014, Additive Particle Deposition and Selective Laser Processing – A Computational Manufacturing Framework, Computational Mechanics, 54:171–191.
[52] Joseph, D.D., Preziosi, L., 1989, Heat Waves, Reviews of Modern Physics, 61: 41–74.